Journal of Controlled Release 355 (2023) 406–416

Contents lists available at ScienceDirect

Journal of Controlled Release

journal homepage: www.elsevier.com/locate/jconrel

Lipid nanoparticle-based ribonucleoprotein delivery for *in vivo* genome editing

Haruno Onuma [1], Yusuke Sato [*,1], Hideyoshi Harashima [*]

Laboratory for Molecular Design of Pharmaceutics, Faculty of Pharmaceutical Sciences, Hokkaido University, Hokkaido, Japan

ARTICLE INFO

Keywords:
Genome editing
Ribonucleoprotein
Lipid nanoparticles
Single stranded oligonucleotides
Melting temperature
Liver

ABSTRACT

The clustered regularly interspaced short palindromic repeats (CRISPR)-associated (Cas) system is a technology that is used to perform site-specific gene disruption, repair, and the modification of genomic DNA *via* DNA repair mechanisms, and is expected to be a fundamental therapeutic strategy for the treatment of infectious diseases and genetic disorders. For clinical applications, the non-viral vector-based delivery of the CRISPR/Cas ribonucleoprotein (RNP) is important, but the poor efficiency of delivery and the lack of a practical method for its manufacture remains as an issue. We report herein on the development of a lipid nanoparticle (LNP)-based Cas RNP delivery system based on optimally designed single stranded oligonucleotides (ssODNs) that allow efficient *in vivo* genome editing. The formation of sequence-specific RNP-ssODN complexes was found to be important for the functional delivery of RNP. Furthermore, the melting temperature (Tm) between sgRNA and ssODN had a significant effect on *in vivo* gene knockout efficiency. An ssODN with a high Tm resulted in limited knockout (KO) activity while that at near room temperature showed the highest KO activity, indicating the importance of the cytosolic release of RNPs. Two consecutive intravenous injections of the Tm optimized formulation achieved approximately 70% and 80% transthyretin KO at the DNA and protein level, respectively, without any obvious toxicity. These findings represent a significant contribution to the development of safe *in vivo* CRISPR/Cas RNP delivery technology and its practical application in genome editing therapies.

1. Introduction

Since 2012, the clustered regularly interspaced short palindromic repeats (CRISPR)-associated (Cas) system has been the subject of much research due to its simplicity of design and the experimental methods needed [1]. Most of the current clinical trials of gene editing therapies involve *ex vivo* gene editing, in which the therapeutic effect is achieved by transplanting cells that had previously been edited *in vitro* into patients [2]. *Ex vivo* gene editing is advantageous in terms of efficacy as well as safety because precisely edited cells can be expanded and used. However, its application is limited to certain specific cells such as hematopoietic stem cells (HSC) and preparing these cells is a costly and complicated task. On the other hand, *in vivo* gene editing, in which the therapeutic effect is achieved by directly introducing genome editing tools to patients either locally or systemically, is considered to be a promising therapeutic strategy for the treatment of genetic diseases, since a simple administration of a therapeutic drug can provide fundamental treatment.

The lipid nanoparticle (LNP) is non-viral and chemically-synthesized delivery system that has been widely studied for use in nucleic acid delivery, and it is currently being used in three approved RNA-based therapies [3]. In 2021, the first clinical trial of CRISPR/Cas genome editing therapy using an LNP were conducted [4]. NTLA-2001, a unique lipid nanoparticle containing an sgRNA targeting transthyretin (TTR) and mRNA encoding *Streptococcus pyogenes Cas9* (spCas9), was used to treat patients with TTR amyloidosis and an 87% reduction in serum TTR levels was achieved after a single injection at a dosage of 0.3 mg/kg.

There are three methods for delivering the CRISPR/Cas system, namely, Cas9-encoded plasmid DNA (pDNA), mRNA or RNP [5]. In the case of the delivery of pDNA or mRNA, the long-term presence of Cas9 protein or gRNA in the cell increases the possibility of off-target effects [6]. Moreover, the long-term presence of the Cas9 protein may cause unnecessary double-stranded breaks (DSBs) in DNA, resulting in potentially harmful effects. Lots of DSBs has been reported to cause chromothripsis and activate p-53 to induce cancer [7,8]. Therefore, methods for delivering guide RNA (gRNA)-Cas9 protein complex (RNP)

* Corresponding authors.
E-mail addresses: y_sato@pharm.hokudai.ac.jp (Y. Sato), harasima@pharm.hokudai.ac.jp (H. Harashima).
[1] These authors contributed equally to this work.

https://doi.org/10.1016/j.jconrel.2023.02.008
Received 25 August 2022; Received in revised form 2 February 2023; Accepted 4 February 2023
Available online 10 February 2023

and genome editing technologies that do not induce DSBs such as base editor, prime editor, RNA editor, CRISPR activation (CRISPRa) or CRISPR interference (CRISPRi), and epigenome editor are also in progress [9–20]. In the case of delivering RNP, the RNPs that are released in the cytosol can induce DNA cleavage through only one step, nuclear transfer, which would permit many inefficient processes in case of delivering pDNA and mRNA to be circumvented [21]. In addition, off-target editing and harmful effects of DSBs could be reduced because RNPs are only transiently present in the cells [22].

RNP delivery shows promise for efficient and safe genome editing, but there are many challenges that need to be addressed, including high cytotoxicity, loading efficiency, release efficiency, stability, and endosomal escape efficiency [23]. In order to solve these ploblems, many *in vivo* RNP delivery systmems are currently being examined and reports of *in vivo* gene editing, including genome editing in the liver and lung by selective organ targeting (SORT) LNPs have recently appeared [24]. Many limitations such as low editing efficacy, low encapsulation efficacy and high toxicity still remain with regard to the current *in vivo* RNP delivery systems.

We report herein on the development of a lipid nanoparticle (LNP)-based Cas RNP delivery system based on the optimal design of single stranded oligonucleotides (ssODNs) that allow efficient *in vivo* genome editing to be performed. The formation of sequence-specific RNP-ssODN complexes was found to be important for the functional delivery of RNP. In addition, the melting temperature (Tm) between sgRNA and ssODN had a significant effect on *in vivo* gene knockout efficiency. The ssODN with a high Tm resulted in limited knockout (KO) activity while that with a Tm near room temperature showed the highest KO activity, indicating the importance of the cytosolic release of RNPs. Two consecutive intravenous injections of the Tm optimized formulation achieved an approximately 70% and 80% transthyretin KO at the DNA and protein level, respectively, without any obvious toxicity.

2. Materials and methods

2.1. Materials

pH-sensitive cationic lipids, CL4H6, was synthesized as described previously [25]. Chol was purchased from SIGMA Aldrich (St. Louis, MO). 1,2-Distearoyl-*sn-glycero*-3-phosphocholine (DSPC), 1,2-dioleoyl-*sn*-glycero-3-phosphoethanolamine (DOPE), and 2-dimirystoyl-*rac*-glycero, methoxyethyleneglycol 2000 ether (PEG-DMG) were obtained from the NOF Corporation (Tokyo, Japan). Recombinant spCas9 nuclease (TrueCut Cas9 Protein v2) was purchased from Thermo Fisher Scientific (MA, USA). Single-guide RNA (sgRNA) and single-stranded oligodeoxynucleotides (ssODNs) were purchased from Integrated DNA Technologies, Inc. (Coralville, IA, USA). A microfluidic device, an iLiNP device, was fabricated as described in a previous report.

2.2. Preparation of RNP-loaded LNPs

A solution of Cas protein (10 μM) was titrated to an equal volume of sgRNA solution (10 μM) under vigorous mixing to produce 5 μM of an RNP solution. The RNP solution was mixed with an equal volume of an ssODN solution (5 μM) to obtain 2.5 μM of RNP-ssODN complex. For the fluorescent labeling of the Cas9 proteins, the RNP-ssON solution was mixed with a 3× molar amount of DyLight 650 NHS ester in DMSO and the resulting solution was then incubated in the dark for 30 min at ambient temperature. Unreacted DyLight 650 was removed by ultrafiltration using an Amicon Ultra-0.5 (MWCO 3 kDa, Millipore). An ethanol solution containing a pH-sensitive cationic lipid, a phospholipid, chol, and PEG-DMG at 50/10/40/3.5 M ratio was prepared at a concentration of 8 mM total lipid. The RNP-ssODN was diluted to 160 nM in 20 mM MES buffer (pH 6.0, 50 mM NaCl). RNP-loaded LNPs were prepared by mixing the lipids in ethanol and RNP-ssODN (approximately equivalent to 5 wt% of the RNP/lipid) in an aqueous solution using an iLiNP device at a total flow rate of 0.5 mL/min (0.050 mL/min for the lipid solution and 0.450 mL/min for the RNP-ssODN solution). Syringe pumps (Harvard apparatus, MA, USA) were used to control the flow rate. The resulting LNP solution was dialyzed for 2 h or more at 4 °C against PBS (−) using Spectra/Por 4 dialysis membranes (molecular weight cut-off 12–14 kDa, Spectrum Laboratories, CA, USA) and was then concentrated by ultrafiltration using Amicon Ultra-15 (MWCO 100 kDa, Millipore).

2.3. Characterization of the LNPs

The size (ζ-average), polydispersity index (PdI) and ζ-potential of the LNPs were measured by means of a Zetasizer Nano ZS ZEN3600 instrument (Malvern Instruments, Worchestershire, UK). The LNPs were diluted in D-PBS(−) and 10 mM HEPES buffer at pH 7.4 for size and ζ-potential measurements, respectively. The encapsulation efficiency (% encapsulation) and total concentration of RNP-ssODN were measured by a Ribogreen assay.

2.4. Measurement of TTR KO activity

BALB/c mice (male, 4 weeks old) were intravenously injected with Cas9/sgTTR RNP-loaded LNPs at the indicated dose. The mice were euthanized one week after the injection, and blood was collected, and serum was isolated by centrifugation. The TTR protein concentration in serum was determined using a Prealbumin ELISA Kit (mouse) (Aviva Systems Biology, CA, USA) according to manufacturer's protocol.

2.5. Evaluation of biodistribution

BALB/c mice were intravenously injected with DyLight 650-labelled LNPs at a dose of 2 mg RNP/kg. At 1 h after the administration, blood was collected and diluted with a 1% sodium dodecyl sulfate (SDS) solution. Tissues were also collected, weighed and homogenized using a Micro Smash MS-100R (TOMY Seiko Co., Ltd.) in a 1% SDS solution. The resulting homogenates were transferred to black 96-well plates and the fluorescence was measured using an VarioskanLux (Thermo Fisher Scientific, MA, USA) with settings of λ_{ex} = 652 nm, λ_{em} = 672 nm. A standard curve was prepared using the LNP solution and blood or tissue homogenates from untreated mice. Biodistribution was expressed as the percentage of the injected dose (%injected dose) per tissue or blood.

2.6. In vitro DNA cleavage activity

Purified genomic DNA (gDNA) was obtained from BALB/c mouse liver tissues using a NucleoSpin Tissue (MACHEREY-NAGEL GmbH & Co. KG) according to the manufacturer's protocol. The dsDNA from TTR locus was amplified by PCR using KAPA HiFi HotStart DNA polymerase (KAPA Biosystems) and was purified using an ISOSPIN PCR Product (Nippon Gene Co., Ltd.). The ssODN (5 equiv. against RNP) was added to TTR targeting Cas9 RNP to form RNP-ssODN complex. The RNP-ssODN complex and the purified PCR product (0.2 equiv. against RNP) was mixed in reaction buffer (50 mM Tris-HCl, 100 mM NaCl. 10 mM $MgCl_2$, 1 mM DTT, pH 7.9) and incubated for 8 h at 37 °C for 30 min or 15 °C (final RNP concentration: 31 nM). After heat inactivation of the Cas9 RNP at 65 °C for 5 min, 50 ng of the dsDNA was run in 3% agarose gel at 100 V for 40 min, stained with GelRed (Biotium, Inc) and visualized with a Printgraph CMOS I (ATTO Corporation). The bands were quantified using the Image J software. DNA cleavage was calculated using the following formula:

$$\text{DNA cleavage} = Int_{cleaved} / Int_{full+cleaved}$$

where Int_{full} and $Int_{cleaved}$ indicate intensity derived from full length (uncleaved) and cleaved DNA, respectively.

2.7. Measurement of the polarization of ssODNs

A 20 nt 5'-FAM-labelled ssODN (1 equiv. against RNP) was added to TTR or GFP targeting Cas9 RNP to form an RNP-ssODN complex. The RNP-ssODNs were diluted to 25 nM in D-PBS(−). These mixtures (100 μL) were transferred to black 96-well plates and incubated at 25 °C or 37 °C for 10 min, and the fluorescence was measured using an infinite 200Pro (Tecan Group Ltd.) with settings of $\lambda_{ex} = 485$ nm, $\lambda_{em} = 535$ nm. The degree of polarization was calculated using the following formula:

$$P = \frac{I_{VV} - GI_{VH}}{I_{VV} + GI_{VH}}$$

$$G = 1.220$$

$$\Delta P = P(RNP - ssODN) - P(ssODN)$$

$$\Delta P' = \Delta P(TTR) - \Delta P(GFP)$$

where VV denotes vertical excitation and vertical emission, VH denotes vertical excitation and horizontal emission, the grating factor, G, is an instrumental correction factor, ΔP and ΔP' indicate the change in polarizability of the ssODNs in the absence and presence of RNPs, and variation of the ssODN polarization by the sgRNA sequence (*i.e.* sequence-dependency), respectively.

2.8. Measurement of Tm of RNP-ssODN complex

The 20 nt 3'-IowaBlack™FQ (IBFQ)-labelled ssODN (5 equiv. against RNP) was added to TTR targeting Cas9 RNP with 5'-FAM-labelled sgRNA (final RNP concentration: 2.5 μM) to form RNP-ssODN complex. The resulting solution (10 μL) was incubated at 10 °C and the temperature was then increased by 1 °C at 10 s intervals using a Thermal Cycler Dice® Real Time System III (TaKaRa Bio Inc., Shiga, Japan). The fluorescence intensity was measured at each temperature from 11 to 70 °C. The temperature at which the fluorescence intensity reached a maximum was defined as the measured Tm.

2.9. T7E1 assay

BALB/c mice (male, 4 weeks old) were intravenously injected with Cas9/sgTTR-G211 RNP-loaded LNPs at a dose of 2 mg RNP/kg for 2 consecutive days. At 1 week after the last injection, the mice were euthanized, and liver tissues were collected, snap frozen in liquid nitrogen and stored at −80 °C.

Purified gDNA was obtained from BALB/c mouse liver tissues using a NucleoSpin Tissue (MACHEREY-NAGEL GmbH & Co. KG) according to manufacturer's protocol. T7E1 assays were performed using an Alt-R® Genome Editing Detection Kit (Integrated DNA technologies, Inc.). The T7E1 treated dsDNA was run in 3% agarose gel at 100 V for 40 min, stained with GelRed (Biotium, Inc) and visualized with a Printgraph CMOS I (ATTO Corporation). The bands were quantified using the Image J software. DNA cleavage was calculated using the following formula:

$$\text{DNA cleavage} = Int_{cleaved} / Int_{full+cleaved}$$

where Int_{full} and $Int_{cleaved}$ indicate intensity derived from full length (uncleaved) and cleaved DNA, respectively.

2.10. Statistical analysis

Results are expressed as the mean ± the SD of independent experiments. For comparisons between the means of two variables, unpaired Student's *t*-tests were performed. For comparisons between multiple groups, one-way analysis of variance (ANOVA) followed by the Student–Newman–Keuls *post hoc* tests or Dunnett's test were performed.

3. Results

3.1. ssODN design strategy

In this study, single-stranded oligonucleotide (ssODN) complexes with sgRNA in RNP *via* base pairing formation, which imparts a negative charge to the RNP and enhances its efficient loading onto the LNPs through electrostatic interactions. However, the strong binding of ssODNs to sgRNAs may inhibit the binding of RNP to the target DNA, possibly reducing genome editing efficiency (Fig. 1A). Actually, in our previous report, a 20 nt-long ssODN that is fully complementary to the sgRNA nearly completely suppressed target gene KO in a cultured cell system [26]. In addition, oligonucleotide inhibitors targeting sgRNA have also been developed to suppress the off-target effects of Cas9 [27]. These findings suggest that the ability of the ssODNs to dissociate from RNPs in the cells is an important factor. Since RNP transfection efficiency increases in a ssODN chain length-dependent manner, as found in our previous study, we used a relatively long ssODN (132 nt) in this study. In addition, in our previous study, we adopted ssODNs, that consisted of sequences that match the genomic DNA containing the target sequence of the sgRNA, to avoid the risk of unintended genetic modification, but such a design is accompanied by the risk that ssODNs could form various secondary structures with each sequence having a different thermodynamic stability. The ssODN design has the potential to cause inconsistent physical properties and transfection efficiency of the LNP formulation among the different sgRNAs. Therefore, we conducted the following two design strategies for the optimal ssODN sequence. First, the sequences at both ends of the ssODN, except for the region complementary to the sgRNA (20 nt in the middle), were changed from a genomic sequence to a polyadenine (poly(A)) sequence to avoid the unintended formation of secondary structures involving the sequences at both ends of the molecule. Both cytidine and guanine were not used because of concerns regarding nonspecific binding to endogenous RNAs due to their strong base pairing ability. Thymine (T) was also not used because of concerns about interactions with the poly(A) sequences in endogenous mRNAs. Second, the thermal stability of the heteroduplex formation between ssODN and sgRNA was reduced to appropriate levels by replacing the mismatched bases at both ends of the complementary region with sgRNA. The mismatched bases were designated adenine (A) if the corresponding sgRNA base was not uridine (U), and T if it was U. Based on this strategy, we designed 7 ssODNs with various complementation rates (0–100%) corresponding to the previously reported TTR-targeting sgRNA (sgTTR-G211) and poly(A) ssODN as a negative control (Fig. 1B) [28]. Tm, an indicator of the binding stability between ssODN and sgRNA, was then calculated. The most commonly used methods for the calculation of Tm include the Wallace method, the GC% method, and the nearest neighbor method. The nearest neighbor method uses thermodynamic parameters and provides relatively accurate results for PCR primer design. However, while the concentration of Na^+ is in the equation assuming a PCR reaction solution, the electrolyte composition in the cytoplasm is very different and more complex than that, so the accuracy would be greatly reduced. The Wallace method, the simplest calculation method, was adopted in this study. The calculated Tm for ssODNs with complementation rates of 30% to 100% was from 20 to 62 °C (Table 1).

3.2. Physicochemical properties of RNP-LNPs

In this study, RNP-loaded LNPs were synthesized using a microfluidic device, and were composed of CL4H6, DSPC, cholesterol, and PEG-DMG at molar ratio of 50/10/40/3.5 (Fig. 2). CL4H6 is a pH-sensitive cationic lipid that was developed in our previous study, and it showed efficient gene disruption in HeLa-GFP cells [25,26].

ζ-Average of RNP-loaded LNPs with each ssODN were 120 to 140 nm (Table 1). The LNP with poly(A) was comparatively large (181 nm at ζ-average) and heterogeneous (PdI > 0.4). LNPs were aggregated when

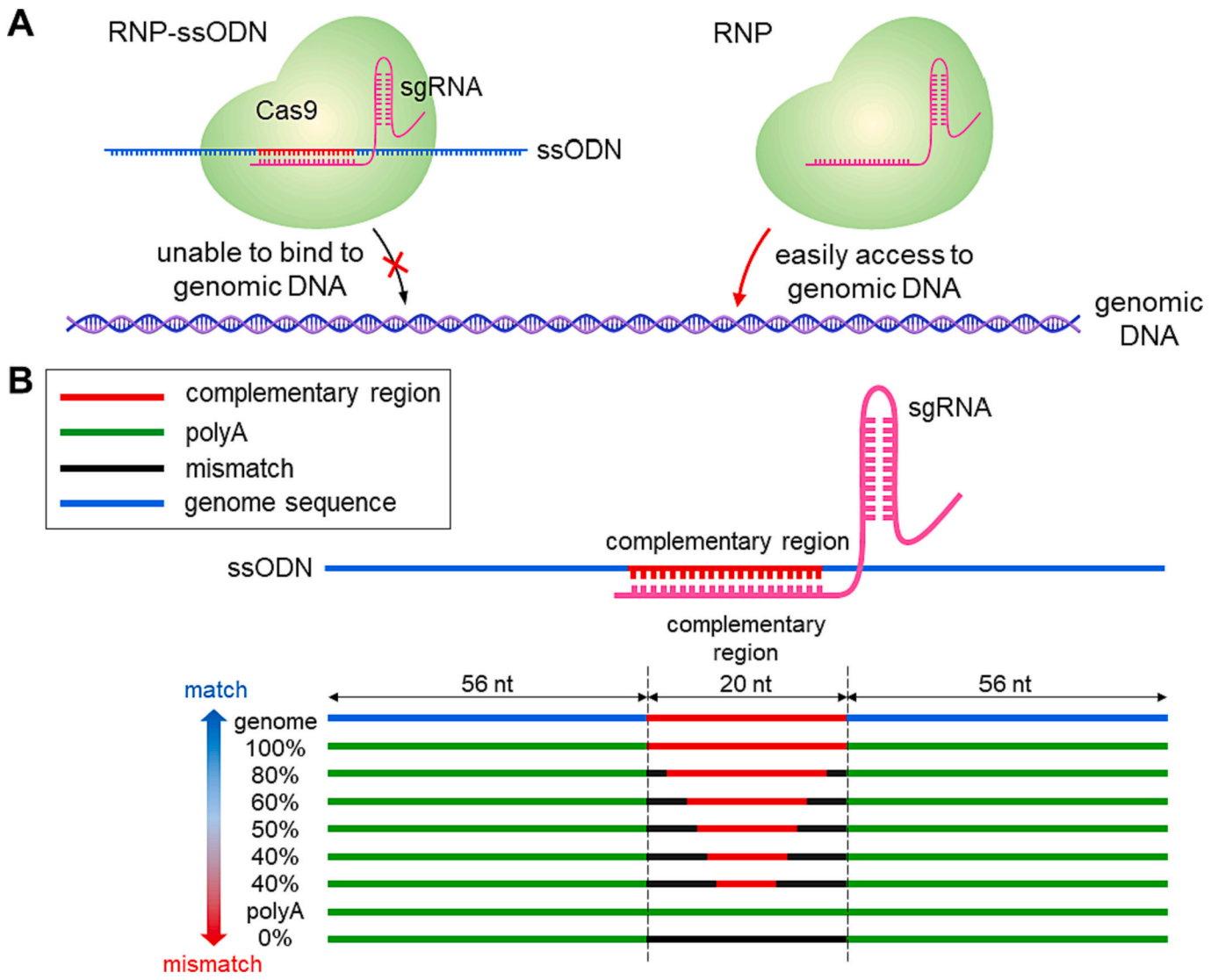

Fig. 1. Strategy for the design of ssODN. (A) Predicted target genomic DNA binding of RNP-ssODN complexes. (B) Schematic illustration of design of ssODN sequences.

Table 1
Calculated Tm of ssODNs and physicochemical properties of RNP-LNPs.

sgRNA	ssODN	Tm (°C) (calculated)	%Encapsulation	ζ average (nm)	PdI	ζ potential (mV)	Recovery ratio (%)
G211	genome	62	41.6	140	0.082	2.3	86.9
	100%	62	70.5	127	0.100	−0.9	74.9
	80%	50	74.9	127	0.127	3.1	76.6
	60%	38	75.4	124	0.165	2.5	87.8
	50%	32	66.6	132	0.225	−1.8	108.1
	40%	26	78.9	140	0.198	2.7	91.2
	30%	20	72.8	121	0.176	0.6	113.4
	polyA	–	82.2	181	0.478	1.3	101.0
	0%	–	84.1	130	0.233	2.9	98.4
	–	–	−8.0	231	0.608	3.4	94.4
G269	80%	48	69.4	110	0.111	3.0	89.4
	60%	36	73.5	150	0.238	1.3	105.7
	50%	30	77.5	134	0.100	1.1	99.5
	40%	24	78.3	136	0.199	1.8	105.8
	30%	18	78.9	139	0.197	1.9	103.4

ssODN was not used. Thus, the formation of sequence-specific RNP-ssODN complexes is important for the synthesis of size-controlled homogenous RNP-loaded LNPs. Regarding RNP encapsulation, LNPs with ssODN with poly(A) at both ends showed higher encapsulation ratios from 66 to 84% in a complementation rate-independent manner while an LNP with the ssODN of the genomic DNA sequence was found to be 42%. The result indicates that avoiding secondary structure formation is important for the efficient s of RNPs into LNPs. It should also be noted,

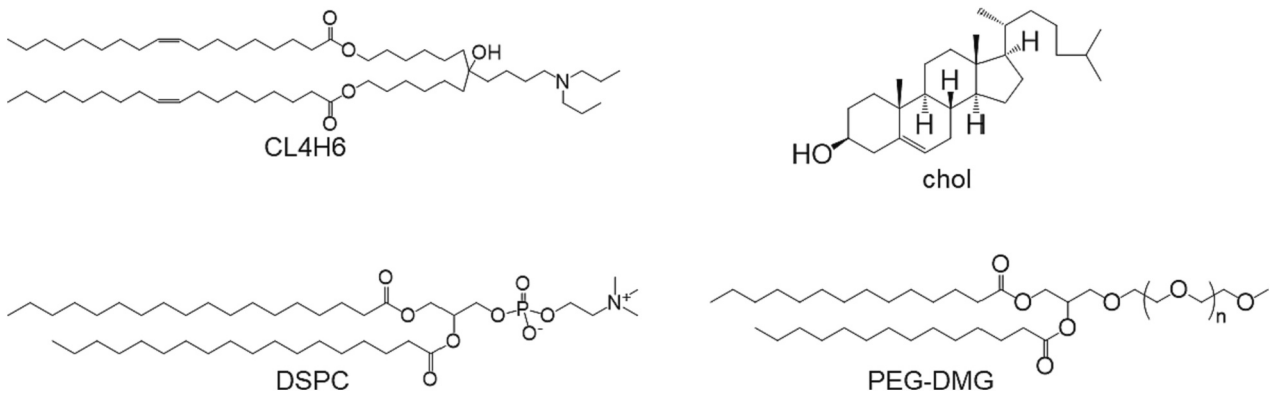

Fig. 2. Chemical structure of the lipids in the LNP.

however, that the RNP encapsulation ratio was measured by detecting nucleic acids using Ribogreen and not the Cas9 protein. Quantification of the encapsulation ratio of Cas9 proteins and evaluation of their localization in LNPs are beyond the scope of this study and are issues that need to be addressed in the future. The ζ-potential of the LNPs was near neutral. Recovery ratio of nucleic acids were 75% at a minimum, suggesting no significant loss of RNPs had occurred during their preparation. We used another TTR-targeting sgRNA (sgTTR-G269) and designed ssODNs with a complementation rate of 30–80% (calculated Tm: 18–48 °C). The physicochemical properties of the LNPs were similar to those with sgTTR-G211, and no clear difference in physical properties were observed between ssODNs with different complementation rates.

3.3. Evaluation of TTR KO activity in vivo

RNP-loaded LNPs were administered intravenously to mice at a dose of 2 mg RNP/kg, and TTR protein levels in serum were quantified 1 week after the administration. For sgTTR-G211, the LNP with 40% complementary ssODN (calculated Tm: 26 °C) suppressed TTR the highest (56%), and for sgTTR-G269, a 50% complementary ssODN (calculated Tm: 30 °C) suppressed TTR the highest (34%) (Fig. 3A). Therefore, for both sgRNAs (TTR-G211, G269), an ssODN with a Tm near room temperature (25 to 30 °C) showed the highest KO activity. On the other hand, LNPs with ssODNs with Tm values at some distance from the appropriate Tm range showed significantly lower KO activity. These results indicate that the Tm of ssODN had a significant impact on the *in vivo* KO activity (Fig. 3B). Given the fact that Tm-dependent KO activity was observed in two different sgRNAs, we conclude that this is a general feature rather than an sgRNA-specific feature. The KO activity of LNPs with a 30% complementary ssODN (calculated Tm: 20 °C) were similar to that with 40% complementary ssODN (calculated Tm: 26 °C) in the case where the LNPs were formulated by using a cooled RNP solution at 4 °C (Fig. S1). This finding suggests that the formation of sequence-specific RNP-ssODN complexes during formulation is important for producing potent LNPs. In order to investigate the impact of the location of mismatched bases on KO activity, we further designed ssODNs with mismatched bases at the 3′ or 5′-end of the complementary region of sgTTR-G211 with three Tm values (10, 25 and 50 °C) and examined their TTR KO activity. As a result, ssODNs with a Tm value of 25 °C showed the highest KO activity of the three Tm values (Fig. S2), suggesting that the Tm value of ssODN is a major factor for KO activity regardless of the location of mismatched bases.

A combination of sgTTR-G211 and 40% complementary ssODN was used in the following experiments. The 80% and 0% complementary ssODNs were also used as negative controls because these would show limited dissociation in the cells and a limited formation of sequence-specific RNP-ssODN complexes, respectively.

3.4. Verification of ssODN design strategy

To investigate the effect of the Tm of ssODN on the delivery of RNPs, the biodistribution of the DyLight 650-labelled RNP-loaded LNPs was quantified at 1 h after intravenous administration. Both RNP-loaded LNPs and free RNP migrated mainly to the liver (Fig. 4A). Intrahepatic

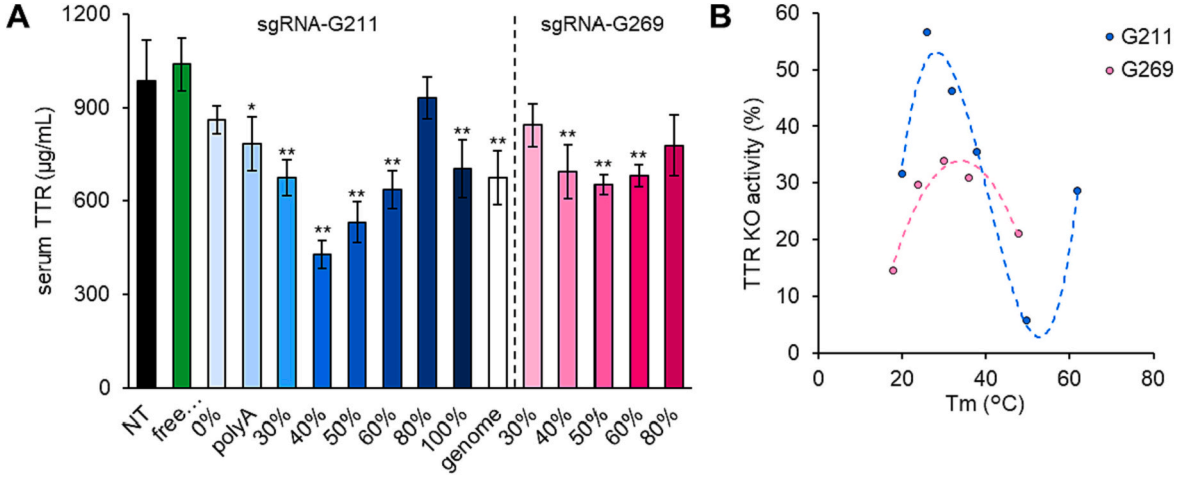

Fig. 3. Evaluation of TTR KO activity *in vivo*. (A) Evaluation of KO activity *in vivo*. RNP-loaded LNPs were administered to BALB/c mice at 2 mg RNP/kg and serum TTR levels were measured 7 days later. $n = 3$–12. $^{*}p < 0.05$, $^{**}p < 0.01$ (Dunnett, *vs.* NT). (B) Relationship between calculated Tm of ssODN and TTR KO activity *in vivo*.

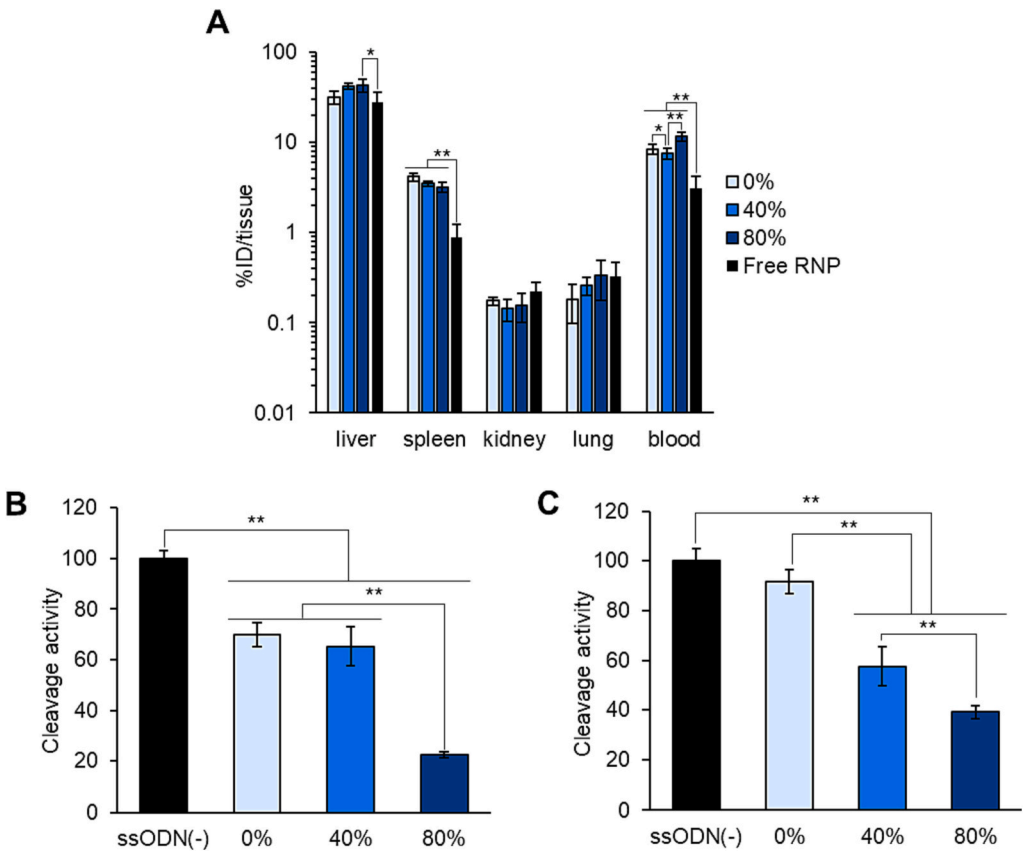

Fig. 4. The biodistribution of RNP-loaded LNPs and the DNA cleavage activity *in vitro*. (A) The biodistribution of LNPs and free RNP. DyLight 650-labelled RNP-loaded LNPs were administered to BALB/c mice at 2 mg RNP/kg. RNPs were quantified 1 h later. $n = 3$. $^{*}p < 0.05$, $^{**}p < 0.01$ (SNK). (B, C) Evaluation of the DNA cleavage activity *in vitro*. (B) RNP-ssODN and the target dsDNA were incubated at 37 °C for 30 min and the cleavage activity then evaluated. n = 3. **p < 0.01 (SNK). (C) RNP-ssODN and the target dsDNA were incubated at 15 °C for 8 h and evaluated the cleavage activity. n = 3. **p < 0.01 (SNK).

observations using confocal laser scanning microscopy (CLSM) revealed that free RNPs were selectively taken up by liver sinusoidal endothelial cells (Fig. S3). Compared to 0% complementary ssODN, both 40% and 80% complementary ssODN tended to accumulate to a greater extent to the liver (no significant difference). On the other hand, the RNP-LNPs accumulated to the spleen compared to the free RNP. As mentioned above, the formation of RNP-ssODN complexes is important for the synthesis of size-controlled LNPs. In other words, if an RNP-ssODN complex does not form, the encapsulation of Cas9 protein inside the LNP is low and Cas9 proteins may be only partially absorbed on the LNP surface. It is possible that the Cas9 protein that was absorbed on the LNP surface is recognized by certain phagocytic cells, thus increasing the amount of migration to the spleen. These findings suggest that the formation of sequence-specific RNP-ssODN complexes is important for achieving hepatic accumulation.

Since *in vivo* experiments showed that the Tm of ssODN had a significant impact on the hepatic delivery of RNPs and TTR KO activity, we then conducted an *in vitro* validation to determine if the ssODN design-based Tm regulation was functional. Cleavage of the target dsDNA was quantified after the incubation of dsDNA and the RNP-ssODN complexes at 37 °C, which mimics temperature *in vivo*. As a result, the cleavage activity of the 80% complementary ssODN was significantly inhibited, while 40% complementary ssODN showed a comparable cleavage activity to the 0% complementary ssODN (Fig. 4B, S4A). This, therefore, suggests that 40% complementary ssODN (calculated Tm: 26 °C) does not interfere with gene KO activity due to its efficient dissociation from RNPs in the cells (~37 °C). On the other hand, the 80% complementary ssODN (calculated Tm: 50 °C) failed to dissociate from the RNPs in the cells and therefore inhibited the binding of RNPs to the target gDNA followed by the induction of gene KO. The decreased cleavage activity in the presence of 0% complementary ssODN compared to free RNP (without ssODN) can be attributed to the sequence-independent adsorption of ssODN on the positively charged Cas9 protein, which potentially inhibits the binding to target dsDNA and/or cleavage activity. As there are high concentrations of endogenous nucleic acids in the cells, the nonspecific adsorption of nucleic acids to Cas9 proteins would occur even in the absence of ssODN. Therefore, in actual cells, the possibility of the inhibition of cleavage activity by the sequence-independent adsorption of 0% complementary ssODN or 40% complementary ssODN co-transfected with RNP is considered to be unlikely.

To verify the temperature dependence of RNP-ssODN complexation, we investigated the target DNA cleavage activity at 15 °C, near or below room temperature, where 40% complementary ssODNs would be expected to complex with the RNPs. The cleavage activity of the 40% complementary ssODN was significantly lower than that of the 0% complementary ssODN (Fig. 4C, S4B), suggesting that 40% complementary ssODN (calculated Tm: 26 °C) can form RNP-ssODN complexes at 15 °C. This result suggests that the formation and dissociation of sequence-specific RNP-ssODN complexes was a temperature-dependent process.

The formation and dissociation of the RNP-ssODN complex was verified by measuring polarization using 5'-FAM-labelled ssODN (Fig. 5A). The difference between the polarizabilities P of ssODN itself and RNP-ssODN complexes was taken as ΔP. The faster the rotation of FAM, the smaller is the polarizability P. Therefore, a larger ΔP indicates the efficient binding of ssODN to RNP. In this experiment, 20 nt ssODNs excluding the poly(A) regions at both ends were used so that FAM rotational kinetics would reflect the binding of ssODNs to RNPs. For sgRNA, in addition to sgTTR, which forms a complementary strand with ssODN, sgGFP, which has an unrelated sequence, was used as a negative control. The difference in ΔP for each sgRNA was defined as ΔP'. For the 80% complementary ssODN, a large change in polarizability between ssODN and RNP-ssODN occurred only for sgTTR (ΔP and ΔP' values were highly positive) (Fig. 5B-D). No change in polarizability occurred when 0% complementary ssODN or 40% complementary ssODN or sgGFP was used. Moreover, the ΔP value became smaller with increasing

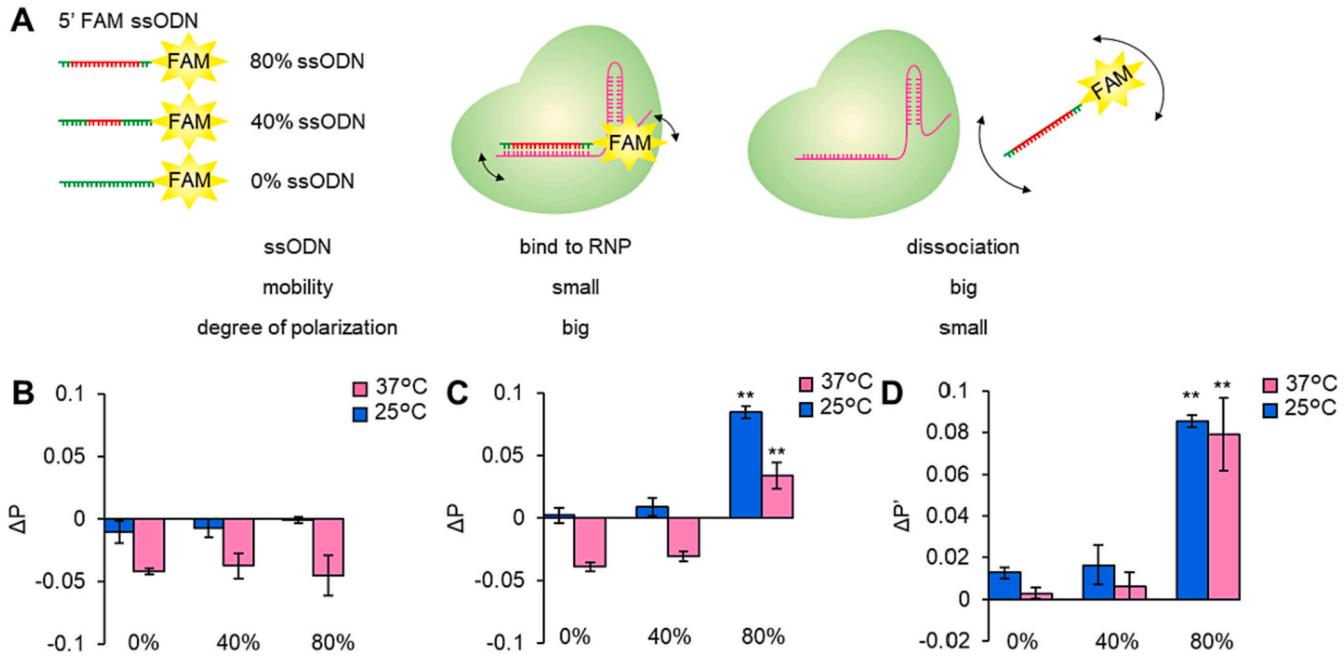

Fig. 5. Measurement of RNP-ssODN mobility using polarimery. (A) Illustration of the experimental system. 20 nt ssODN modified with FAM at the 5′ end was used to measure polarization. (B, C) The difference between the polarizabilities P of ssODN itself and RNP-ssODN was ΔP. (B) ΔP with sgGFP. $n = 3$. $^{**}p < 0.01$ (Dunnett, *vs.* 0%). (C) ΔP with sgTTR. n = 3. **p < 0.01 (*vs.* 0%) (Dunnett). (D) The difference between ΔP of sgGFP and sgTTR was ΔP'. n = 3. **p < 0.01 (Dunnett, *vs.* 0%).

temperature from 25 °C to 37 °C. Therefore, this suggests that the formation and dissociation of sequence-specific RNP-ssODN complexes was temperature-dependent. However, no sequence-dependent difference in mobility was observed for the 40% complementary ssODN, which would be the result of the presence of mismatched bases at the 5′-end of ssODN.

The above polarization experiment failed to detect the formation of RNP-ssODN complexes for 40% complementary ssODN which can be attributed to the unintended high flexibility of FAM due to mismatched bases in ssODN. Thus, we measured the Tm of the RNP-ssODN complex by measuring the difference in distance by fluorescence quenching using 5'-FAM-labelled sgRNA and 3'-IBFQ-labelled ssODN (Fig. 6A). In this experiment, fluorescence is quenched by the proximity of FAM to IBFQ only when ssODN forms a complementary strand with gRNA. In this study, we used 20 nt ssODNs with the poly(A) regions at both ends excluded because the proximity of fluorescence dye and quencher is important for the efficiency of quenching. The fluorescence intensities of FAM for RNP-ssODNs with 0%, 40%, and 80% complementary ssODNs was monitored from 11 to 70 °C. The 40% and 80% complementary ssODNs showed a substantial quenching of FAM at low temperatures and the fluorescence increased with increasing temperature, indicating that the dissociation of ssODNs from RNPs was temperature-dependent (Fig. 6B). The temperature at which the change in fluorescence intensity reached a maximum was defined as the "measured" Tm. The measured Tm was 32 °C and 62 °C for the 40% and 80% complementary ssODN, respectively (Fig. 6C), indicating that 40% complementary ssODN dissociate from RNPs while the 80% complementary ssODN

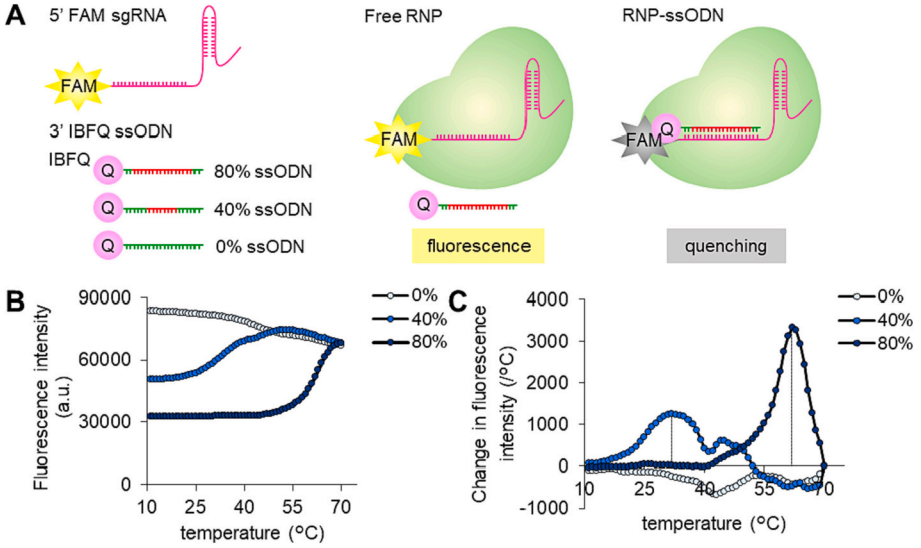

Fig. 6. Verification of the formation of RNP-ssODN complex by fluorescence quenching. (A) Illustration of the experiments. 5'-FAM-labelled sgRNA and 3'-IBFQ-labelled 20 nt ssODN were used to monitor the FAM fluorescence. (B) A plot of fluorescence intensity of FAM against temperature. Fluorescence of FAM was monitored from 11 °C to 70 °C. $n = 3$. (C) Change in FAM fluorescence with temperature change. n = 3.

remained fully bound to RNPs under an *in vivo* environment (~40 °C). These data strongly support the conclusion that dissociation of ssODN from RNP upon being delivered to the cytosol is a critical process for gene KO. Compared to 80% complementary ssODN, the 40% complementary ssODN showed a smaller quenching extent (Fig. 6B). Similar to the polarization experiment, this may be due to the large average distance between FAM and IBFQ because the 40% complementary ssODN has a large number of mismatched bases at the 3′-ends. However, although differences in quenching efficiency were observed between 80% and 40% complementary ssODNs, the formation of an RNP-ssODN could be detected because quenching can occur even when FAM and IBFQ are slightly distanced from one another.

3.5. Evaluation of KO activity in vivo by repeated administration

TTR KO activity of the ssODN-optimized LNPs (sgRNA: sgTTRG211, ssODN: 40% complementary ssODN) was also evaluated. The RNP-LNPs achieved a 56% reduction in serum TTR protein levels after a single administration (Fig. 3A). We then examined the issue of whether its KO effect is cumulative by repeated administration and whether the RNP-LNP is toxic when sufficient KO efficiency is achieved. The RNP-LNPs were intravenously administered at a dose of 2 mg RNP/kg for 2 days. Serum TTR protein levels and editing in the liver were examined at 1 week after the last dose. The results showed that the RNP-loaded LNPs achieved an approximately 80% reduction in serum TTR protein level (Fig. 7A). An approximate indel mutation of 27% was detected by a T7 endonuclease 1 (T7E1) assay (Fig. 7B). Negligible cleavage in the spleen and lung was observed, suggesting that the RNP-loaded LNPs functionally delivered RNPs specifically to the liver (Fig. S5). Furthermore, the NGS showed that 70% of TTR genes in the whole liver were edited (Fig. 7C). Single nucleotide insertion was dominant in the edited reads (Fig. 7D).

The safety of RNP-loaded LNPs was evaluated after consecutive administration. No significant difference in body weight was observed between the LNP and PBS groups (Fig. S6). Analysis of hematological parameters revealed no significant increase in indicators of hepatotoxicity, alanine transaminase (ALT) and aspartate transaminase (AST) (Table 2). The pH-responsive cationic lipid CL4H6 used in this study is known to be rapidly degraded by esterase enzymes and only about 1% remained in the liver after 24 h [25]. Therefore, we conclude that the

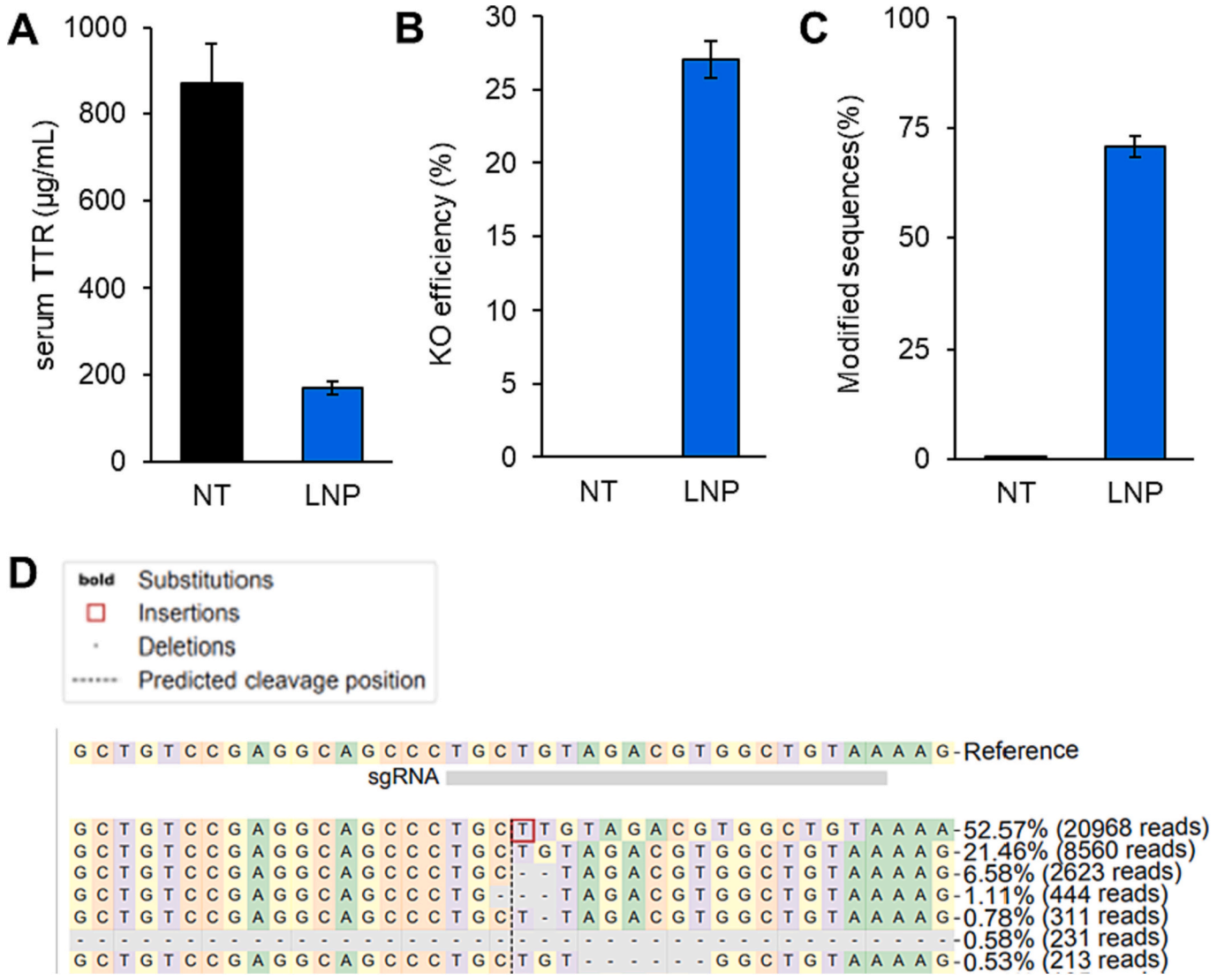

Fig. 7. Evaluation of KO activity *in vivo* by the repeated administration of RNP-loaded LNPs. (A) RNP-loaded LNPs were intravenously administered to BALB/c mice at a dose of 2 mg RNP/kg on two consecutive days, and serum TTR levels were measured 7 days after the last dose. $n = 3$. (B) DNA extracted from the liver was evaluated by a T7E1 assay. n = 3. (C) Editing efficiency in the liver measured by NGS. n = 3. (D) The top seven alleles around the cleavage site in the LNP-treated group.

Table 2
Hematology of the administered RNP-LNP on consecutive days.

Parameters	PBS	LNP	Parameters	PBS	LNP
TP (g/dL)	4.7 ± 0.2	4.63 ± 0.05	ALT (IU/L)	30.0 ± 1.6	26.7 ± 1.2
ALB (g/dL)	3.3 ± 0.2	3.13 ± 0.05	LDH (IU/L)	620.7 ± 49.4	944.0 ± 468.5
BUN (mg/dL)	27.0 ± 0.9	20.27 ± 2.18*	AMY (IU/L)	2391.3 ± 111.9	2300.3 ± 86.3
CRE (mg/dL)	0.1 ± 0	0.117 ± 0.005*	γ-GT (IU/L)	< 3	< 3
Na (mEq/L)	151.3 ± 0.5	149.7 ± 0.5*	T-CHO (mg/dL)	80.0 ± 5.9	87.3 ± 2.5
K (mEq/L)	4.2 ± 0.7	4.2 ± 0.3	TG (mg/dL)	107.7 ± 15.2	74.7 ± 5.9*
Cl (mEq/L)	109.0 ± 0.8	107 ± 0.8	HDL-C (mg/dL)	48.0 ± 2.9	51.0 ± 1.6
Ca (mg/dL)	8.8 ± 0.3	8.4 ± 0.2	T-BIL (mg/dL)	0.06 ± 0.03	0.07 ± 0.02
IP (mg/dL)	9.6 ± 0.6	10.4 ± 0.7	GLU (mg/dL)	158.7 ± 4.2	169.3 ± 15.2
AST (IU/L)	72.3 ± 8.4	77.3 ± 6.3			

TP: total protein, ALB: albumin, BUN: blood urea nitrogen, CRE: creatinine, IP: inorganic phosphates, AST: aspartate transaminase, ALT: alanine transaminase, LDH: lactose dehydrogenase, AMY: amylase, γ-GT: gamma-glutamyl transpeptidase, T-CHO: total cholesterol, TG: triglyceride, HDL—C: high density lipoprotein cholesterol, T-BIL: total bilirubin, GLU: glucose. n = 3. *$p < 0.05$ (*vs.* PBS).

RNP-loaded LNPs are quite safe and that this is due to the high biodegradability of the CL4H6 that is used in the formulation.

4. Discussion

In this study, the formation of sequence-specific RNP-ssODN complexes was found to be important for the encapsulation of RNP into an LNP and their migration to the target organ. In parallel, the efficient dissociation of ssODN from RNP was critical for cleaving the target gDNA by the RNPs. Therefore, the design of ssODNs that form and dissociate sequence-specific complexes in a temperature dependent manner should be a useful strategy for efficient *in vivo* genome editing by enabling both complex formation during manufacture and intracellular dissociation. In previous reports regarding the delivery of RNPs by DNA Nanoclew, the authors indicated that the partial complementation of Nanoclew and sgRNA was important for the efficient delivery of RNP and the induction of efficient KO activity, but there is no report that focused on the optimum complementation and Tm of ssODN and sgRNA [29,30]. In this study, we established a method of determining the optimum complementation of ssODN for specific sgRNAs by designing ssODNs based on Tm regulation. Moreover, this strategy is a versatile strategy that can be applied to other RNP delivery carriers. Therefore, it represents one useful approach to the current challenges of RNP delivery by non-viral vectors, such as low loading efficiency and low stability *in vivo*. The development of a selective organ targeting (SORT) LNP allowed genome editing to be achieved, not only in the liver but also in the lung by the delivery of RNP [24]. Combining this strategy is also expected to achieve efficient genome editing in non-liver tissue.

In this study, we found a large difference in the KO activity of two sgRNAs (TTRG211, TTRG269), which showed comparable activity in a previous report (Fig. 3A) [28]. In the CRISPR/Cas system, RNPs need to unravel the DNA double helix when searching for target sequences, and their cleavage activity has been reported to be greatly reduced in the less accessible heterochromatin regions [31–33]. Since the previous report used CD-1 mice whereas BALB/c mice were used in the present study, the difference in activity of the two sgRNAs may be due to differences in nucleosome occupancy of the target sequence between the mice strains.

The fully (100%) complementary ssODN of sgTTR-G211 showed a higher KO activity compared to the 80% complementary ssODN (Fig. 3A). ssODN forms a secondary structure by intramolecular base pairing based on hydrogen bonding in a sequence-dependent manner [34]. The substantial activity of the 100% complementary ssODN of sgTTR-G211 can be attributed to the presence of self-complementary sequences within the ssODN, which may contribute to destabilizing the formation of complementary strands with sgRNA (lower Tm), which is not accounted for in the Wallace method. The secondary structure of the 100% complementary ssODN was predicted using the Mfold online server (http://www.unafold.org/) (Fig. S7) [35]. However, these results were only predictions, and it is not possible to consider the complicated environment *in vivo*. Therefore, although it is difficult to quantitatively evaluate the impact of the secondary structure of ssODNs at this time, this is a future task to be addressed. The 0% complementary ssODN and polyA showed a low KO activity in spite of their high encapsulation efficiencies (Fig. 3A, Table 1).

The ssODNs with the mismatched bases at the 3′ or 5′-end of the complementary region with sgRNA showed a high KO activity compared to the ssODNs with mismatched bases at both ends of the complementary region (Fig. S2). In particular, the 25 °C-3′ and 25 °C-5’ ssODN showed TTR KO activity that was comparable to that for the repeated administration of 40% ssODN (Tm 26 °C) with mismatched bases at both ends of the complementary region. This suggests that KO activity is affected, not only by the Tm value of ssODN but also the location of mismatched bases. The location of mismatched bases may affect the formation of secondary structures of ssODNs, the encapsulation of Cas9 proteins and the internal structure of RNP-LNPs. This represents a subject that should be investigated in a future study.

The RNP-LNP with 0% complementary ssODN was significantly heterogeneous compared with 40% and 80% complementary ssODNs (Fig. S8). This suggests that the formation of sequence-specific RNP-ssODN complexes can impart negative charges directly to the RNPs, therefore contributing to the synthesis of homogenous RNP-LNPs. Therefore, it is probable that the internal structure (*e.g.* the distribution of RNPs in LNP) of RNP-LNP with 0% complementary ssODN differs from RNP-LNPs with ssODNs which have a high complementary ratio. The difference in internal structure could affect the stability of RNP-LNPs *in vivo*, such as binding to blood proteins and the efficiency of delivery to the target cells, which may be one of the reasons for the low KO activity of the 0% complementary ssODN and polyA. However, we failed to identify any differences in these RNP-LNPs by evaluating the encapsulation efficiencies, so it is important to evaluate the encapsulation efficiency of the Cas9 protein and to examine the structure of RNP-LNPs in the future.

The KO activity, as evaluated by a T7E1 assay, was lower than that evaluated by ELISA and NGS. Of the indels induced by the RNP-loaded LNP, 71% were insertions of T. However, as the T7E1 enzyme cannot recognize single nucleotide mutations, the KO activity evaluated by a T7E1 assay was significantly lower than the values for the other two analyses [36,37]. The indels induced by spCas9 are most commonly associated with single nucleotide insertions [38]. In a preclinical study of mRNA-LNP (NTLA-2001) in Caique monkeys using CRISPR/Cas, which is currently undergoing clinical trials, 99% of the mutations that occurred were T insertions, and the results of our study are also consistent with this finding [4].

By the repeated administration of RNP-LNPs, we achieved an approximately 80% reduction in the serum levels of the TTR protein (Fig. 7A). TTR is the causative gene in familial amyloid polyneuropathy (FAP) and a target of FDA-approved nucleic acid-based medicines such as patisiran and inotersen, which show promising therapeutic effects by reducing serum TTR protein level [39,40]. These medicines have shown clinical effects by an approximately 80% reduction in serum TTR protein levels (patisiran: 81%, inotersen: 74%). Therefore, the double administration of the RNP-LNPs is expected to have considerable potential for achieving therapeutic effects.

In this study, because both ends of the ssODN are poly(A) to avoid

secondary structure formation, knock-in by homologous recombination (HR) using the ssODN as a template is not possible. Our current strategy ensures the consistency of the physicochemical properties of LNPs, the efficiency of the introduction of RNPs, and the intracellular dynamics of RNPs in the delivery of RNP aimed gene knockout. It is possible to induce the knock-in of a short fragment or base substitution by using ssODN with homology arms, as was demonstrated in our previous report [26]. On the other hand, gene knock-in utilizing HR is difficult to apply for non-dividing cells that make up most of the somatic cells in the body because HR is known to occur only in the late S and G2 phases of the cell cycle [41]. Gene knock-in methods such as Precise Integration into Target Chromosome (PITCh) system utilizing microhomology-mediated end-joining (MMEJ) and homology-independent targeted integration (HITI) system utilizing non-homologous end joining (NHEJ) have been reported recently [42,43]. In the future, these methods could be applied to RNP-loaded LNP to achieve highly efficient gene knock-in by a completely artificial non-viral delivery system.

Further modification of ssODN can also be considered. In this study, both ends of the ssODN are poly(A), but it is possible that ssODNs, which form compact higher-order structures only at both ends, may increase the efficiency of incorporation of RNP into LNPs. The possibility of unintended genetic recombination occuring due to the use of ssODNs that differ from the genomic DNA sequence is also a concern. Since both ends of ssODN are poly(A), the possibility of genetic recombination is very low in consideration of the affinity, but this was not verified in detail in this study. In our previous report, we reported on the successful efficient delivery and induction of gene knockout by complexing ssRNA with both spCas9 and Cpf1 RNPs [26]. The use of ssRNA as a negative charge to RNPs enable the risk of unintended genetic recombination to genomic DNA to be avoided and the safety of genome editing with RNP-loaded LNPs to be improved.

A further prospect is the development of optimal lipids for RNP delivery. In this study, we used pH-responsive cationic lipids (CL4H6) that were identified in a study of siRNA delivery [25]. It is possible that cationic lipids suitable for the delivery of RNPs with complex properties and diffuse charges on protein surfaces may be very different from those that are suitable for siRNAs and mRNAs. It is quite possible that the gene knockout activity of RNP-loaded LNP could be further enhanced by developing cationic lipids that are more suitable for efficient RNP delivery.

5. Conclusions

In this study, we report on a method for determining the optimal complementation rate of ssODN for the *in vivo* delivery of any sgRNA CRISPR/Cas RNPs by designing ssODNs based on Tm regulation. By adding mismatches to ssODN based on Tm regulation, we succeeded in both RNP-ssODN complex formation during formulation and dissociation in the cell. The ssODN-optimized formulation was shown to induce robust gene disruption *in vivo* without any apparent toxicity. These findings represent a significant contribution to the development of safe *in vivo* CRISPR/Cas RNP delivery technology and its practical application in genome editing therapies.

CRediT authorship contribution statement

Haruno Onuma: Formal analysis, Investigation, Writing – original draft, Visualization. **Yusuke Sato:** Conceptualization, Methodology, Validation, Formal analysis, Investigation, Resources, Writing – original draft, Writing – review & editing, Supervision, Funding acquisition. **Hideyoshi Harashima:** Writing – review & editing, Supervision, Funding acquisition.

Declaration of Competing Interest

The authors declare the following competing financial interest(s): H. Onuma, Y. Sato, and H. Harashima have filed intellectual property related to this publication.

Data availability

Data will be made available on request.

Acknowledgements

This work was supported, in part, by the Special Education and Research Expenses from the Ministry of Education, Culture, Sports, Science and Technology, Hokkaido University Support Program for Frontier Research, and TERUMO LIFE SCIENCE FOUNDATION. The authors also wish to thank Dr. Milton S. Feather for his helpful advice in preparing the English manuscript.

Appendix A. Supplementary data

Supplementary data to this article can be found online at https://doi.org/10.1016/j.jconrel.2023.02.008.

References

[1] M. Jinek, K. Chylinski, I. Fonfara, M. Hauer, J.A. Doudna, E. Charpentier, A programmable dual-RNA-guided DNA endonuclease in adaptive bacterial immunity, Science 337 (2012) 816–821.
[2] J.M. Lim, H.H. Kim, Basic principles and clinical applications of CRISPR-based genome editing, Yonsei Med. J. 63 (2022) 105–113.
[3] Y. Zhang, C. Sun, C. Wang, K.E. Jankovic, Y. Dong, Lipids and lipid derivatives for RNA delivery, Chem. Rev. 121 (2021) 12181–12277.
[4] J.D. Gillmore, E. Gane, J. Taubel, J. Kao, M. Fontana, M.L. Maitland, J. Seitzer, D. O'Connell, K.R. Walsh, K. Wood, J. Phillips, Y. Xu, A. Amaral, A.P. Boyd, J. E. Cehelsky, M.D. McKee, A. Schiermeier, O. Harari, A. Murphy, C.A. Kyratsous, B. Zambrowicz, R. Soltys, D.E. Gutstein, J. Leonard, L. Sepp-Lorenzino, D. Lebwohl, CRISPR-Cas9 in vivo gene editing for transthyretin amyloidosis, N. Engl. J. Med. 385 (2021) 493–502.
[5] Y. Lin, E. Wagner, U. Lächelt, Non-viral delivery of the CRISPR/Cas system: DNA, Biomater. Sci. 10 (2022) 1166–1192.
[6] X. Liang, J. Potter, S. Kumar, Y. Zou, R. Quintanilla, M. Sridharan, J. Carte, W. Chen, N. Roark, S. Ranganathan, N. Ravinder, J.D. Chesnut, Rapid and highly efficient mammalian cell engineering via Cas9 protein transfection, J. Biotechnol. 208 (2015) 44–53.
[7] M.L. Leibowitz, S. Papathanasiou, P.A. Doerfler, L.J. Blaine, L. Sun, Y. Yao, C. Z. Zhang, M.J. Weiss, D. Pellman, Chromothripsis as an on-target consequence of CRISPR-Cas9 genome editing, Nat. Genet. 53 (2021) 895–905.
[8] O.M. Enache, V. Rendo, M. Abdusamad, D. Lam, D. Davison, S. Pal, N. Currimjee, J. Hess, S. Pantel, A. Nag, A.R. Thorner, J.G. Doench, F. Vazquez, R. Beroukhim, T. R. Golub, U. Ben-David, Cas9 activates the p53 pathway and selects for p53-inactivating mutations, Nat. Genet. 52 (2020) 662–668.
[9] N.M. Gaudelli, A.C. Komor, H.A. Rees, M.S. Packer, A.H. Badran, D.I. Bryson, D. R. Liu, Programmable base editing of a•T to G•C in genomic DNA without DNA cleavage, Nature 551 (2017) 464–471.
[10] A.C. Komor, Y.B. Kim, M.S. Packer, J.A. Zuris, D.R. Liu, Programmable editing of a target base in genomic DNA without double-stranded DNA cleavage, Nature 533 (2016) 420–424.
[11] E.B. Esrick, L.E. Lehmann, A. Biffi, M. Achebe, C. Brendel, M.F. Ciuculescu, H. Daley, B. MacKinnon, E. Morris, A. Federico, D. Abriss, K. Boardman, R. Khelladi, K. Shaw, H. Negre, O. Negre, S. Nikiforow, J. Ritz, S.Y. Pai, W. B. London, C. Dansereau, M.M. Heeney, M. Armant, J.P. Manis, D.A. Williams, Post-transcriptional genetic silencing of, N. Engl. J. Med. 384 (2021) 205–215.
[12] A.V. Anzalone, P.B. Randolph, J.R. Davis, A.A. Sousa, L.W. Koblan, J.M. Levy, P. J. Chen, C. Wilson, G.A. Newby, A. Raguram, D.R. Liu, Search-and-replace genome editing without double-strand breaks or donor DNA, Nature 576 (2019) 149–157.
[13] D. Böck, T. Rothgangl, L. Villiger, L. Schmidheini, M. Matsushita, N. Mathis, E. Ioannidi, N. Rimann, H.M. Grisch-Chan, S. Kreutzer, Z. Kontarakis, M. Kopf, B. Thöny, G. Schwank, In vivo prime editing of a metabolic liver disease in mice, Sci. Transl. Med. 14 (2022) eabl9238.
[14] T. Stafforst, M.F. Schneider, An RNA-deaminase conjugate selectively repairs point mutations, Angew. Chem. Int. Ed. Eng. 51 (2012) 11166–11169.
[15] P. Monian, C. Shivalila, G. Lu, M. Shimizu, D. Boulay, K. Bussow, M. Byrne, A. Bezigian, A. Chatterjee, D. Chew, J. Desai, F. Favaloro, J. Godfrey, A. Hoss, N. Iwamoto, T. Kawamoto, J. Kumarasamy, A. Lamattina, A. Lindsey, F. Liu, R. Looby, S. Marappan, J. Metterville, R. Murphy, J. Rossi, T. Pu, B. Bhattarai, S. Standley, S. Tripathi, H. Yang, Y. Yin, H. Yu, C. Zhou, L.H. Apponi, P. Kandasamy, C. Vargeese, Endogenous ADAR-mediated RNA editing in non-human primates using stereopure chemically modified oligonucleotides, Nat. Biotechnol. 40 (2022) 1093–1102.

[16] D. Katrekar, J. Yen, Y. Xiang, A. Saha, D. Meluzzi, Y. Savva, P. Mali, Efficient in vitro and in vivo RNA editing via recruitment of endogenous ADARs using circular guide RNAs, Nat. Biotechnol. 40 (2022) 938–945.
[17] L.A. Gilbert, M.H. Larson, L. Morsut, Z. Liu, G.A. Brar, S.E. Torres, N. Stern-Ginossar, O. Brandman, E.H. Whitehead, J.A. Doudna, W.A. Lim, J.S. Weissman, L. S. Qi, CRISPR-mediated modular RNA-guided regulation of transcription in eukaryotes, Cell 154 (2013) 442–451.
[18] H. Park, Y. Hwang, J. Kim, Transcriptional activation with Cas9 activator nanocomplexes rescues Alzheimer's disease pathology, Biomaterials 279 (2021), 121229.
[19] J.K. Nuñez, J. Chen, G.C. Pommier, J.Z. Cogan, J.M. Replogle, C. Adriaens, G. N. Ramadoss, Q. Shi, K.L. Hung, A.J. Samelson, A.N. Pogson, J.Y.S. Kim, A. Chung, M.D. Leonetti, H.Y. Chang, M. Kampmann, B.E. Bernstein, V. Hovestadt, L. A. Gilbert, J.S. Weissman, Genome-wide programmable transcriptional memory by CRISPR-based epigenome editing, Cell 184 (2021) 2503–2519.e2517.
[20] M.P. Gemberling, K. Siklenka, E. Rodriguez, K.R. Tonn-Eisinger, A. Barrera, F. Liu, A. Kantor, L. Li, V. Cigliola, M.F. Hazlett, C.A. Williams, L.C. Bartelt, V.J. Madigan, J.C. Bodle, H. Daniels, D.C. Rouse, I.B. Hilton, A. Asokan, M. Ciofani, K.D. Poss, T. E. Reddy, A.E. West, C.A. Gersbach, Transgenic mice for in vivo epigenome editing with CRISPR-based systems, Nat. Methods 18 (2021) 965–974.
[21] S. Kim, D. Kim, S.W. Cho, J. Kim, J.S. Kim, Highly efficient RNA-guided genome editing in human cells via delivery of purified Cas9 ribonucleoproteins, Genome Res. 24 (2014) 1012–1019.
[22] M.A. DeWitt, J.E. Corn, D. Carroll, Genome editing via delivery of Cas9 ribonucleoprotein, Methods 121-122 (2017) 9–15.
[23] M. Behr, J. Zhou, B. Xu, H. Zhang, Delivery of CRISPR-Cas9 therapeutics: Progress and challenges, Acta Pharm. Sin. B 11 (2021) 2150–2171.
[24] T. Wei, Q. Cheng, Y.L. Min, E.N. Olson, D.J. Siegwart, Systemic nanoparticle delivery of CRISPR-Cas9 ribonucleoproteins for effective tissue specific genome editing, Nat. Commun. 11 (2020) 3232.
[25] Y. Sato, K. Hashiba, K. Sasaki, M. Maeki, M. Tokeshi, H. Harashima, Understanding structure-activity relationships of pH-sensitive cationic lipids facilitates the rational identification of promising lipid nanoparticles for delivering siRNAs in vivo, J. Control. Release 295 (2019) 140–152.
[26] Y. Suzuki, H. Onuma, R. Sato, Y. Sato, A. Hashiba, M. Maeki, M. Tokeshi, M.E. H. Kayesh, M. Kohara, K. Tsukiyama-Kohara, H. Harashima, Lipid nanoparticles loaded with ribonucleoprotein-oligonucleotide complexes synthesized using a microfluidic device exhibit robust genome editing and hepatitis B virus inhibition, J. Control. Release 330 (2020) 61–71.
[27] C.L. Barkau, D. O'Reilly, K.J. Rohilla, M.J. Damha, K.T. Gagnon, Rationally designed anti-CRISPR nucleic acid inhibitors of CRISPR-Cas9, Nucleic. Acid Ther. 29 (2019) 136–147.
[28] J.D. Finn, A.R. Smith, M.C. Patel, L. Shaw, M.R. Youniss, J. van Heteren, T. Dirstine, C. Ciullo, R. Lescarbeau, J. Seitzer, R.R. Shah, A. Shah, D. Ling, J. Growe, M. Pink, E. Rohde, K.M. Wood, W.E. Salomon, W.F. Harrington, C. Dombrowski, W.R. Strapps, Y. Chang, D.V. Morrissey, A single administration of CRISPR/Cas9 lipid nanoparticles achieves robust and persistent in vivo genome editing, Cell Rep. 22 (2018) 2227–2235.
[29] W. Sun, W. Ji, J.M. Hall, Q. Hu, C. Wang, C.L. Beisel, Z. Gu, Self-assembled DNA nanoclews for the efficient delivery of CRISPR-Cas9 for genome editing, Angew. Chem. Int. Ed. Eng. 54 (2015) 12029–12033.
[30] W. Sun, J. Wang, Q. Hu, X. Zhou, A. Khademhosseini, Z. Gu, CRISPR-Cas12a delivery by DNA-mediated bioresponsive editing for cholesterol regulation, Sci. Adv. 6 (2020) eaba2983.
[31] R.M. Yarrington, S. Verma, S. Schwartz, J.K. Trautman, D. Carroll, Nucleosomes inhibit target cleavage by CRISPR-Cas9 in vivo, Proc. Natl. Acad. Sci. U. S. A. 115 (2018) 9351–9358.
[32] M.A. Horlbeck, L.B. Witkowsky, B. Guglielmi, J.M. Replogle, L.A. Gilbert, J. E. Villalta, S.E. Torigoe, R. Tjian, J.S. Weissman, Nucleosomes impede Cas9 access to DNA in vivo and in vitro, Elife 5 (2016).
[33] S. Jain, S. Shukla, C. Yang, M. Zhang, Z. Fatma, M. Lingamaneni, S. Abesteh, S. T. Lane, X. Xiong, Y. Wang, C.M. Schroeder, P.R. Selvin, H. Zhao, TALEN outperforms Cas9 in editing heterochromatin target sites, Nat. Commun. 12 (2021) 606.
[34] T.N. Navien, R. Thevendran, H.Y. Hamdani, T.H. Tang, M. Citartan, In silico molecular docking in DNA aptamer development, Biochimie 180 (2021) 54–67.
[35] M. Zuker, Mfold web server for nucleic acid folding and hybridization prediction, Nucleic Acids Res. 31 (2003) 3406–3415.
[36] D. Bhattacharya, E.G. Van Meir, A simple genotyping method to detect small CRISPR-Cas9 induced indels by agarose gel electrophoresis, Sci. Rep. 9 (2019) 4437.
[37] L. Vouillot, A. Thélie, N. Pollet, Comparison of T7E1 and Surveyor Mismatch Cleavage Assays to Detect Mutations Triggered by Engineered Nucleases, G3 (Bethesda) vol. 5, 2015, pp. 407–415.
[38] F. Allen, L. Crepaldi, C. Alsinet, A.J. Strong, V. Kleshchevnikov, P. De Angeli, P. Páleníková, A. Khodak, V. Kiselev, M. Kosicki, A.R. Bassett, H. Harding, Y. Galanty, F. Muñoz-Martínez, E. Metzakopian, S.P. Jackson, L. Parts, Predicting the mutations generated by repair of Cas9-induced double-strand breaks, Nat. Biotechnol. 37 (2018) 64–72.
[39] D. Adams, A. Gonzalez-Duarte, W.D. O'Riordan, C.C. Yang, M. Ueda, A.V. Kristen, I. Tournev, H.H. Schmidt, T. Coelho, J.L. Berk, K.P. Lin, G. Vita, S. Attarian, V. Planté-Bordeneuve, M.M. Mezei, J.M. Campistol, J. Buades, T.H. Brannagan, B. J. Kim, J. Oh, Y. Parman, Y. Sekijima, P.N. Hawkins, S.D. Solomon, M. Polydefkis, P.J. Dyck, P.J. Gandhi, S. Goyal, J. Chen, A.L. Strahs, S.V. Nochur, M.T. Sweetser, P.P. Garg, A.K. Vaishnaw, J.A. Gollob, O.B. Suhr, Patisiran, an RNAi therapeutic, for hereditary transthyretin amyloidosis, N. Engl. J. Med. 379 (2018) 11–21.
[40] M.D. Benson, M. Waddington-Cruz, J.L. Berk, M. Polydefkis, P.J. Dyck, A.K. Wang, V. Planté-Bordeneuve, F.A. Barroso, G. Merlini, L. Obici, M. Scheinberg, T. H. Brannagan, W.J. Litchy, C. Whelan, B.M. Drachman, D. Adams, S.B. Heitner, I. Conceição, H.H. Schmidt, G. Vita, J.M. Campistol, J. Gamez, P.D. Gorevic, E. Gane, A.M. Shah, S.D. Solomon, B.P. Monia, S.G. Hughes, T.J. Kwoh, B. W. McEvoy, S.W. Jung, B.F. Baker, E.J. Ackermann, M.A. Gertz, T. Coelho, Inotersen treatment for patients with hereditary transthyretin amyloidosis, N. Engl. J. Med. 379 (2018) 22–31.
[41] S.A. Smirnikhina, M.I. Zaynitdinova, V.A. Sergeeva, A.V. Lavrov, Improving homology-directed repair in genome editing experiments by influencing the cell cycle, Int. J. Mol. Sci. 23 (2022).
[42] S. Nakade, T. Tsubota, Y. Sakane, S. Kume, N. Sakamoto, M. Obara, T. Daimon, H. Sezutsu, T. Yamamoto, T. Sakuma, K.T. Suzuki, Microhomology-mediated end-joining-dependent integration of donor DNA in cells and animals using TALENs and CRISPR/Cas9, Nat. Commun. 5 (2014) 5560.
[43] K. Suzuki, Y. Tsunekawa, R. Hernandez-Benitez, J. Wu, J. Zhu, E.J. Kim, F. Hatanaka, M. Yamamoto, T. Araoka, Z. Li, M. Kurita, T. Hishida, M. Li, E. Aizawa, S. Guo, S. Chen, A. Goebl, R.D. Soligalla, J. Qu, T. Jiang, X. Fu, M. Jafari, C.R. Esteban, W.T. Berggren, J. Lajara, E. Nuñez-Delicado, P. Guillen, J. M. Campistol, F. Matsuzaki, G.H. Liu, P. Magistretti, K. Zhang, E.M. Callaway, J. C. Belmonte, In vivo genome editing via CRISPR/Cas9 mediated homology-independent targeted integration, Nature 540 (2016) 144–149.